

# Distant Solar System Objects identified in the Pan-STARRS1 survey

R.J. Weryk<sup>1</sup>, E. Lilly<sup>1</sup>

S. Chastel<sup>1</sup>, L. Denneau<sup>1</sup>, R. Jedicke<sup>1</sup>, E. Magnier<sup>1</sup>, R.J. Wainscoat<sup>1</sup>

K. Chambers<sup>1</sup>, H. Flewelling<sup>1</sup>, M.E. Huber<sup>1</sup>, C. Waters<sup>1</sup>

PS1 Builders

Received \_\_\_\_\_; accepted \_\_\_\_\_

32 Pages, 9 Figures, 7 Tables

---

<sup>1</sup>Institute for Astronomy, University of Hawaii, 2680 Woodlawn Drive, Honolulu HI 96822,  
USA

## ABSTRACT

We present a method to identify distant solar system objects in long-term wide-field asteroid survey data, and conduct a search for them in the Pan-STARRS1 (PS1) image data acquired from 2010 to mid-2015. We demonstrate that our method is able to find multi-opposition orbital links, and we present the resulting orbital distributions which consist of 154 Centaurs, 255 classical Trans-Neptunian Objects (TNOs), 121 resonant TNOs, 89 Scattered Disc Objects (SDOs) and 10 comets. Our results show more than half of these are new discoveries, including a newly discovered 19th magnitude TNO. Our identified objects do not show clustering in their argument of perihelia, which if present, might support the existence of a large unknown planetary-sized object in the outer solar system.

**Key Words:** Asteroids, Trans-Neptunian Objects, Centaurs, Orbit Determination, Data reduction techniques

## 1. Introduction

### 1.1. Background and Importance

The minor planets orbiting beyond Neptune provide valuable insight on our solar system’s formation and evolution, but they have only been studied since 1992 when the first Trans-Neptunian Object (TNO) after Pluto was discovered (Jewitt & Luu 1993). Almost a quarter century later,  $\sim 2000$  TNOs and Centaurs are known (see Figure 1) and they are revealing their properties slowly because of the difficulties involved with detecting the faint, slow-moving members of this distant population.

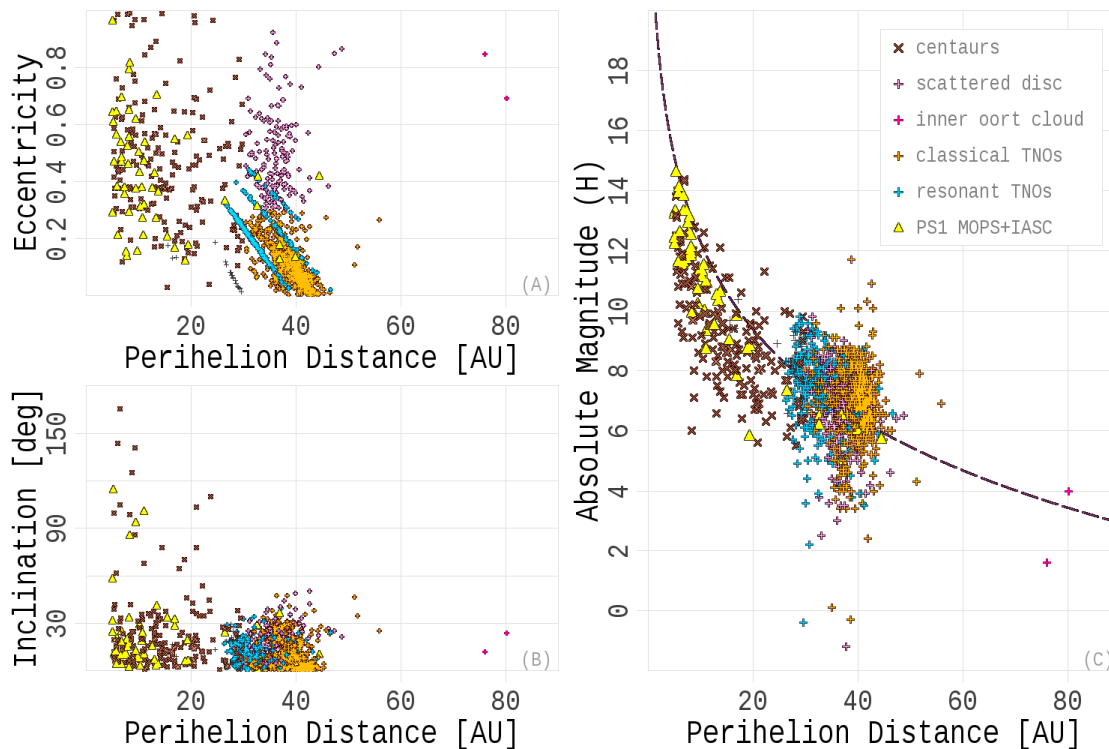


Fig. 1.— (A) Eccentricity, (B) inclination, and (C) absolute magnitude, versus perihelion distance of known TNOs (including SDOs; orange, magenta, and blue marks), Centaurs (brown), and Inner Oort Cloud objects (IOCs; red dots). Objects previously discovered by PS1 through MOPS and IASC (as mentioned in the text) are depicted as yellow triangles. The limiting absolute magnitude is shown as a dashed line in panel (C) for  $V = 22.5$ .

Multiple dedicated TNO surveys have been conducted over the years (e.g., Larsen et al. 2001; Gladman et al. 2001; Bernstein et al. 2004; Elliot et al. 2005; Petit et al. 2006, 2008; Sheppard et al. 2011; Gladman et al. 2012; Alexandersen et al. 2014; Brown et al. 2015) including stellar occultation surveys (e.g., Schlichting et al. 2012) which focussed on the discovery of sub-km objects below the sensitivity limit of optical telescopes. Thanks to these studies, the large 100 – 1000 km objects have a well characterized size-frequency distribution (SFD; Petit et al. 2008; Fuentes & Holman 2008) while TNOs smaller than 100 km have only more recently been studied (Fraser 2009; Sheppard & Trujillo 2010; Gladman et al. 2012). However, there is a need for more observational data to confirm the apparent transition from a steep to shallow SFD slope among the Neptune Trojans (Sheppard & Trujillo 2010) and SDOs (Shankman et al. 2013) around  $D \sim 100$  km (corresponding to absolute magnitude  $H \sim 8.5$ ) (Alexandersen et al. 2014). If the transition is present within all TNO sub-populations it would suggest the formation scenario in which “asteroids were born big” (Morbidelli et al. 2009) and imply that objects smaller than 100 km are dominantly the result of collisional evolution.

Most of the known TNOs were discovered in ‘deep and narrow’ observing campaigns using large telescopes with small fields of view. Current Near Earth Object (NEO) surveys (Larson et al. 1998; Kaiser 2004) have the advantage of continuously monitoring large portions of the sky over several years, but are disadvantaged because they use smaller telescopes with cadences designed to identify NEOs that move more than  $10\times$  faster than TNOs. Brown et al. (2015) searched archival data from the Catalina Sky Survey (Larson et al. 2003) and Siding Spring Survey (Larson et al. 2003) and independently identified the eight brightest known TNOs. Even though they did not discover any new objects they predicted a 32% chance that an object having magnitude  $V < 19.1$  remains undiscovered in the unsurveyed region of the sky.

Evidence has been mounting in the past few years that there is a large planetary-sized distant object in our solar system whose gravitational perturbations influence the orbits of Scattered-Disc Objects (SDOs), particularly those on orbits similar to the dwarf planet (90377) Sedna (e.g., Trujillo & Sheppard 2014; de la Fuente Marcos et al. 2015; Batygin & Brown 2016). These works suggest that all currently known extreme TNOs with semi-major axis greater than 150 AU (including the only other Sedna-like object: 2012 VP<sub>113</sub>) show a pronounced clustering in their arguments of perihelia ( $\omega$ ) not present in the closer TNO population. Trujillo & Sheppard (2014) suggest this clustering is centred at  $\omega \sim 0^\circ$  and that it is due to the Lidov—Kozai effect, a three-body interaction capable of constraining  $\omega$  (Kozai 1962). They propose that a super-Earth mass body located at  $\sim 250$  AU would be capable of restricting  $\omega$  for these objects and be stable for billions of years. However, Batygin & Brown (2016) made a similar calculation, but excluded orbits which do not demonstrate long term stability because of Neptune, and found that the distant TNOs cluster around  $\omega \sim 318^\circ \pm 8^\circ$  which is inconsistent with the Kozai mechanism. They suggest instead that the clustering can be maintained by a distant ten Earth-mass planet on an eccentric orbit with semi-major axis 700 AU, nearly co-planar with the distant TNOs, but with  $\omega$  shifted by  $180^\circ$ . In addition, such a planet might explain the presence of highly inclined TNOs whose existence has not yet been explained (Gladman et al. 2009). Trujillo & Sheppard (2014) also state that another plausible explanation for such a peculiar asymmetric  $\omega$  configuration would be a strong stellar encounter with the Oort cloud in the past.

Increasing the number of known retrograde TNOs and Sedna-like SDOs is needed to further test these hypotheses and to constrain the orbital elements and mass of any potentially undiscovered planet. Towards that end, in this work we report on the discovery and detection of the largest number of TNOs by a single asteroid survey, which due to its long-duration and wide-field coverage, provides an excellent complement to targeted

deep-and-narrow surveys, resulting in a relatively unbiased TNO sample.

## 1.2. Pan-STARRS

The prototype telescope for the Panoramic Survey Telescope and Rapid Response System (Pan-STARRS1, hereafter referred to as PS1) located in the United States on Haleakala, Maui, Hawaii, has been surveying the sky since 2010. Many of the observations by PS1 were taken as a sequence of four exposures, each separated by a Transient Time Interval (TTI) of  $\sim 20$  minutes. This cadence was selected to optimise detection of Near Earth Objects (NEOs) — objects which have perihelia  $q < 1.3$  AU. Observations from each night are rapidly processed by the Image Processing Pipeline (Magnier 2006), and all detected moving objects identified by the Moving Object Processing System (MOPS; Denneau et al. 2013) are reported to the Minor Planet Center. PS1 has become the leading discovery telescope for NEOs, discovering almost half of the new Near Earth Asteroids in 2015, and discovering more than half of the new comets in 2015 (Wainscoat et al. 2015).

The detection of NEOs is done using subtraction of image pairs which have a TTI of  $\sim 20$  minutes and are well matched in image quality and telescope pointing. This TTI spacing produces a lower limit on the rate of motion for detection of moving objects, below which moving objects are self-subtracted in their image pairs. The lower limit is typically  $\sim 0.04^\circ$  per day ( $= 2''$  in 20 minutes), and is seeing dependent. A substantial number of Centaurs (which we define as having perihelia between Jupiter and Neptune) have been discovered from the pair-subtracted images, but only a few more-distant objects have been reported from PS1 (see Figure 1), some of which were discovered via the International Astronomical Search Collaboration (IASC<sup>1</sup>), an educational outreach program in which

---

<sup>1</sup><http://iasc.hsutx.edu/>

images were blinked manually.

Now that PS1 has thoroughly surveyed the sky north of  $-30^\circ$  declination, other methods become viable for object detection that are potentially more sensitive to both fainter and slower moving objects. One method uses subtraction of a high-quality static sky image, derived from the cumulative survey data. The other method uses the historical survey to establish a catalogue of stationary objects, and compares catalogues of new detections in new images to the static sky, to reveal moving objects.

Over the course of the PS1 survey, image quality has improved, but the grid structure in the PS1 CCDs requires many dithered images to produce a clean static sky image. And although good images in the *gri* passbands are now available for much of the sky north of  $-30^\circ$  declination, the coverage in the more sensitive *w* passband is more sparse, because surveying in that band has been more focused on the ecliptic for the purpose of NEO discovery. The PS1 survey has also only recently been extended south to  $-49^\circ$  declination. For these reasons, we have focussed our initial exploration of methods to extract fainter moving objects on the catalogue based approach.

## 2. Methodology

To locate moving sources in the PS1 data, a new search method was developed and run on source catalogues previously generated by the IPP (Magnier 2006) from PS1 images taken between 2010 Feb 24 and 2015 July 31. These catalogues are generated by a source extraction program which identifies and measures the point spread function for objects in the images. A detection is the information recorded about an object in a single exposure, and the catalogues contain detections of moving objects as well as stationary sources which must be removed.

The method, as described in the following sections, links sets of detections (corresponding to the same object) from a single night into a ‘tracklet’. Tracklets from multiple nights which correspond to the same object are then searched for. Figure 2 shows the apparent path across the celestial sphere over four years for a typical TNO. Our method first searches for two related tracklets which are used to generate an initial orbit from which ephemerides are calculated to identify additional tracklets. All detections identified for an object have their image stamps extracted, which are visually inspected to ensure they are real and do not correspond to image artefacts or stationary sources that were not removed.

While the PS1 MOPS pipeline (Denneau et al. 2013) was designed to identify TNOs, it requires a survey pattern and cadence that was not implemented. The method presented here is able to link TNOs using a survey pattern intended for NEO detection.

## 2.1. Stationary Source Identification and Removal

Objects in the outer solar system appear to move slowly across the celestial sphere, with their apparent paths dominated by the motion of Earth. TNOs in a 3:2 mean motion resonance with Neptune, such as Pluto, will have a maximum angular speed at opposition of  $0.022^\circ$  per day, equal to  $3.2''$  per hour for orbits near zero inclination and eccentricity. An object much farther out at 550 AU will move  $0.25''$  (the PS1 pixel scale) in one hour. However, even the most distant objects which move less than the astrometric uncertainty in one night will move a noticeable amount over multiple nights, allowing visual verification that they are indeed moving targets.

To identify stationary sources, consider a specific telescope pointing (defined by the boresight direction and telescope rotation). All source detections for all exposures overlapping the field-of-view at this boresight direction are loaded. For each detection, the



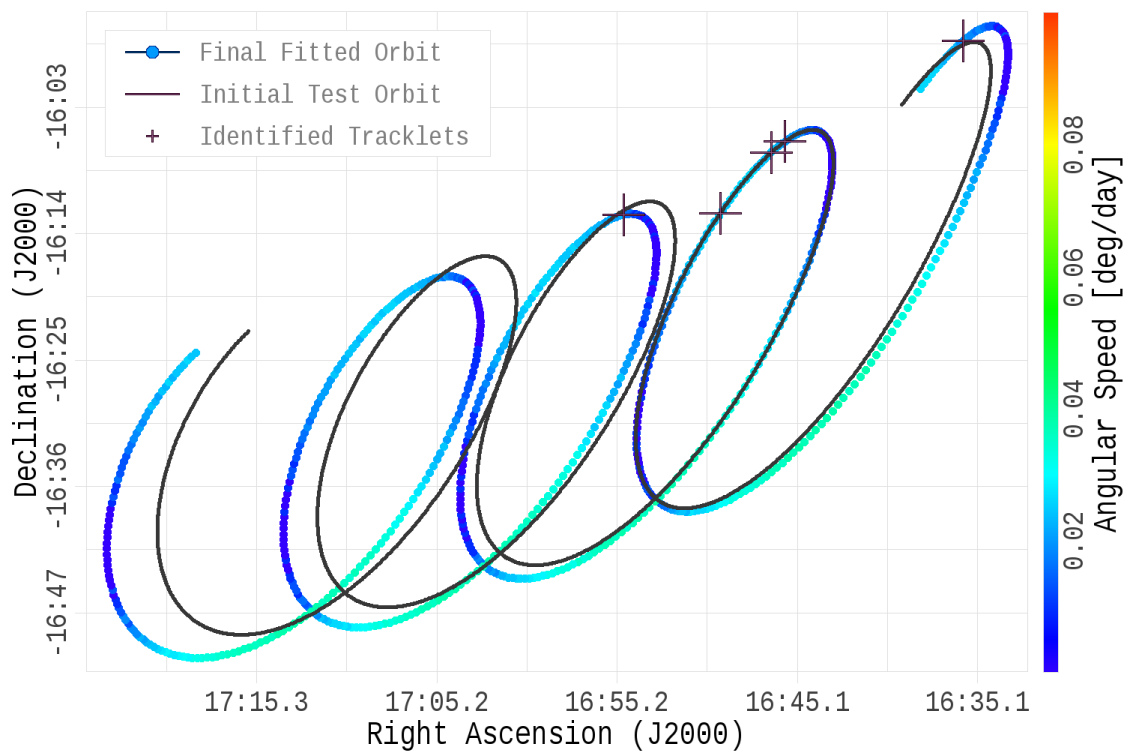


Fig. 2.— The ephemerides of the initial orbit (determined from a tracklet pair) and the final five-tracklet orbit for a sample event. Because the motion cannot be represented with a linear or quadratic projection (the loops are due to the motion of the Earth), a tracklet linking routine based on ephemerides must be used. For this event, the ephemerides from the two orbits differ by  $\sim 9'$  after six months, and by  $\sim 15'$  after one year, which is less than the  $20'$  search radius described in the text.

number of neighbouring detections within two magnitudes and  $0.6''$  are counted. Because each PS1 telescope pointing is typically observed four times in a given night (the average TTI is 19 minutes, giving an average 57 minute arc), we consider a detection stationary if it is present more than four times, i.e., if there are detections at the same location on the celestial sphere within  $0.6''$  over multiple nights. These criteria were determined empirically and relate to the astrometric and photometric uncertainty in the PS1 images.

Once all stationary sources are identified, they are removed from the catalogues. The detections which remain are then used for tracklet creation. Note that while valid detections may be rejected, 100% efficiency is not required as candidate objects are likely to have been observed multiple times at different positions along their orbits.

## 2.2. Tracklet Creation

Tracklets are formed from detections following a procedure similar to the stationary source removal. The detections from all exposures of a given pointing for a single night are loaded and iterated over. All detections within 0.4 magnitudes and  $16''$  from each other are assigned a tracklet number. The choice of  $16''$  means many tracklets for inner Solar System objects will be present in the tracklet dataset, as this corresponds to  $0.43^\circ$  per day for exposures with a TTI of 15 minutes. While these objects can be linked with our algorithm, we exclude any identified object having semi-major axis  $< 4.8$  AU, as we are only interested in objects at heliocentric distances corresponding to Jupiter’s orbit and beyond. While we could use a search distance  $< 16''$ , this choice does allow us to identify tracklets where the second or third detection occurred within a CCD cell gap.

Once formed, each tracklet has its motion along a great circle fit with a constant angular speed model. Only tracklets with RMS residual  $< 0.3''$  and having  $\geq 3$  detections

are kept, and their fitted angular speed and position angle are recorded. We do not create tracklets from detection pairs because we cannot apply an RMS test to judge their astrometric quality. Some fraction of the formed tracklets may be faint stars or image artefacts which exhibit linear motion, and their presence will increase the required computational time since there are more tracklet comparisons to be made. We validate all orbit fits using residual checks.

This linking process is different from the kd-tree based algorithm used by MOPS (Denneau et al. 2013) described in detail by Kubica et al. (2007). The method presented here is computationally faster, but is limited to tracklets moving at much slower speed, and it cannot handle the intersection of tracklets which correspond to detections of different objects with similar apparent magnitude.

### 2.3. Tracklet Pairing

To test if two tracklets correspond to the same object, a brute-force approach is used. All tracklet pairs occurring within up to  $6^\circ$  (equal to the maximum angular speed of  $0.1^\circ$  per day with a 60 day window) have a test orbit fit using FindOrb <sup>2</sup>, and we require its reported mean residual  $< 0.3''$ . The choice of a 60 day window is a trade off between an improved initial arc length, and the computation time needed to test all tracklet pairs, and is reasonable since the PS1 survey pattern has observed much of the celestial sphere on at least three separate nights within this timespan (see Figure 3). However, this method is affected by missed tracklets which may have fallen into CCD cell gaps, been obscured by other image artefacts, or are too close to bright stars. We do not require every tracklet pair for an object to be identified, as many TNOs should be detected in more than two

---

<sup>2</sup>[http://www.projectpluto.com/find\\_orb.htm](http://www.projectpluto.com/find_orb.htm)

tracklets for the timespan considered here (see Figure 3). It is important to note however, that some orbital geometries will not have any observations: for example, there are no PS1 observations of the Centaur (10199) Chariklo which is located near the galactic centre.

To increase computational efficiency, tracklet pairs are identified using a kd-tree indexed approach, and the position angle of both tracklets must be within  $24^\circ$  of a line connecting the two tracklets. This value was empirically chosen and considerably reduces the computation time required as it excludes certain unphysical geometries. We consider only tracklets having angular speed between  $0.1^\circ$  and  $0.001^\circ$  per day, as our priority in this work is to find TNOs. An extended search for more distant objects will be considered in future work.

#### 2.4. Identifying additional tracklets

The search for additional tracklets to extend an object’s arc length requires a starting orbit, for which we use the tracklet pairing results described in the previous section. The metadata for each PS1 exposure is loaded, sorted by the observation time relative to the starting orbit’s epoch (where its mean anomaly is defined), and iterated over. For each exposure, an ephemeris is generated, and if located within the field-of-view, the corresponding tracklet database is searched. For each tracklet which contains detections within  $20'$  of the test ephemeris, a new orbit is fit using FindOrb. If the reported mean residual is  $< 0.2''$ , the tracklet is considered linked, its astrometry appended, and the updated orbit fit kept. The search then continues for additional tracklets. The choice of  $0.2''$  is more strict than the limit used during tracklet pairing, but has identified up to 27 additional tracklets for the candidate objects.

Table 1 shows how the initial test orbit of a sample object converges as additional

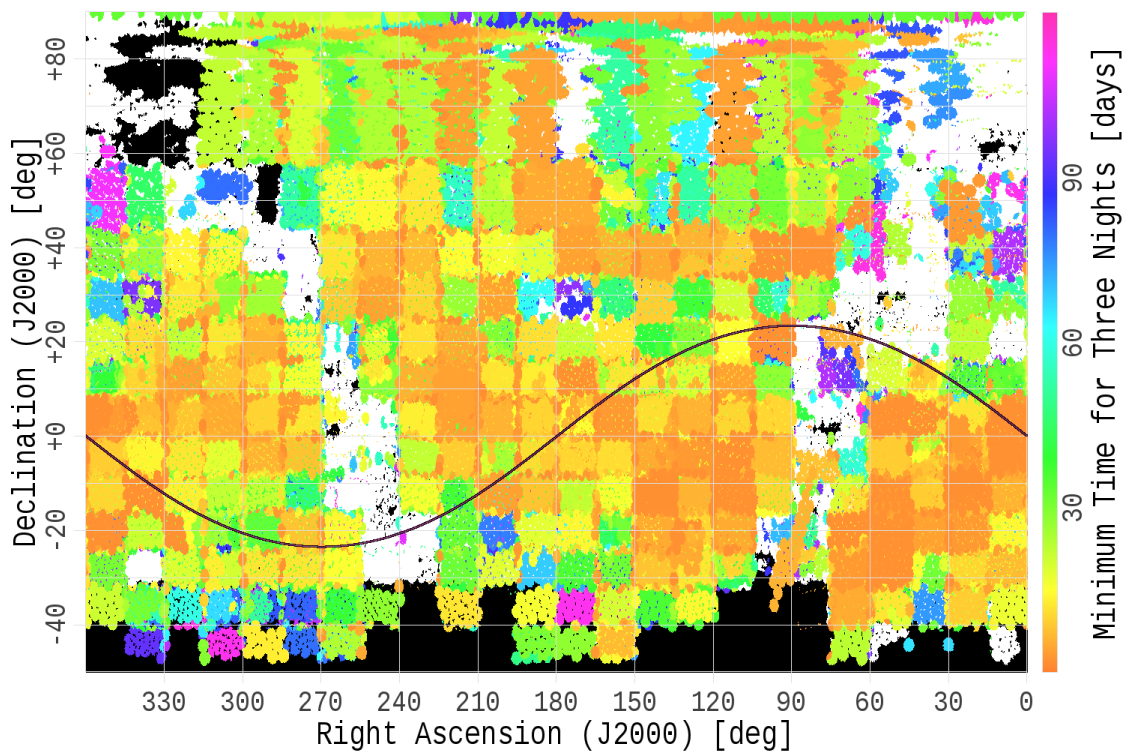


Fig. 3.— Minimum timespan in the PS1 survey to observe the celestial sphere on three separate nights, ignoring observations consisting of only one or two exposures. The block pattern is due to how the survey strategy was implemented. The ecliptic plane is shown as a curved line. Black regions indicate three observations have never been made, while white (mostly corresponding to the galactic plane) means there are more than 120 days between the first and third nights. The majority of the surveyed area satisfies the tracklet pairing search window of 60 days.

Table 1: Typical sample of a classical TNO (with  $H = 6.5$ ) showing how its orbit converges as additional tracklets are found, with five total tracklets being identified. All orbits are integrated to the 20140702.0 epoch used for the initial two-tracklet case. The first column ( $N$ ) in the table is the number of tracklets used to compute the orbit.

$N$	$a$ [AU]	$e$	$i$ [°]	$\omega$ [°]	$\Omega$ [°]	$q$ [AU]	$M$ [°]
2	33.2933	0.0726	7.374	94.233	198.516	30.8756	325.536
3	39.2198	0.2176	7.283	59.306	197.561	30.6844	357.708
4	39.4907	0.2247	7.288	63.932	197.506	30.6186	354.920
5	39.3916	0.2212	7.279	57.769	197.518	30.6778	358.711

tracklets were found. The difference in the ephemeris for the initial and final orbit is illustrated in Figure 2. The choice of the 20' search distance was chosen based on identified TNOs: Figure 4 shows the angular distance between ephemerides from the initial tracklet-pair based orbit and the final fitted orbit for all identified objects. The majority of events show  $< 20'$  difference over  $\pm 120$  days, where (based on Figure 3) most of the celestial sphere has been observed on at least three nights during the PS1 survey.

While we could integrate the test orbits using Mercury6 (Chambers 1999) to account for their orbital evolution, this is not required for TNOs as the generated ephemerides will change by much less than the 20' search distance.

## 2.5. Visual Inspection and Classification

The image stamps for each detection from all identified objects were extracted and visually inspected to confirm they were real and not affected by image artefacts.

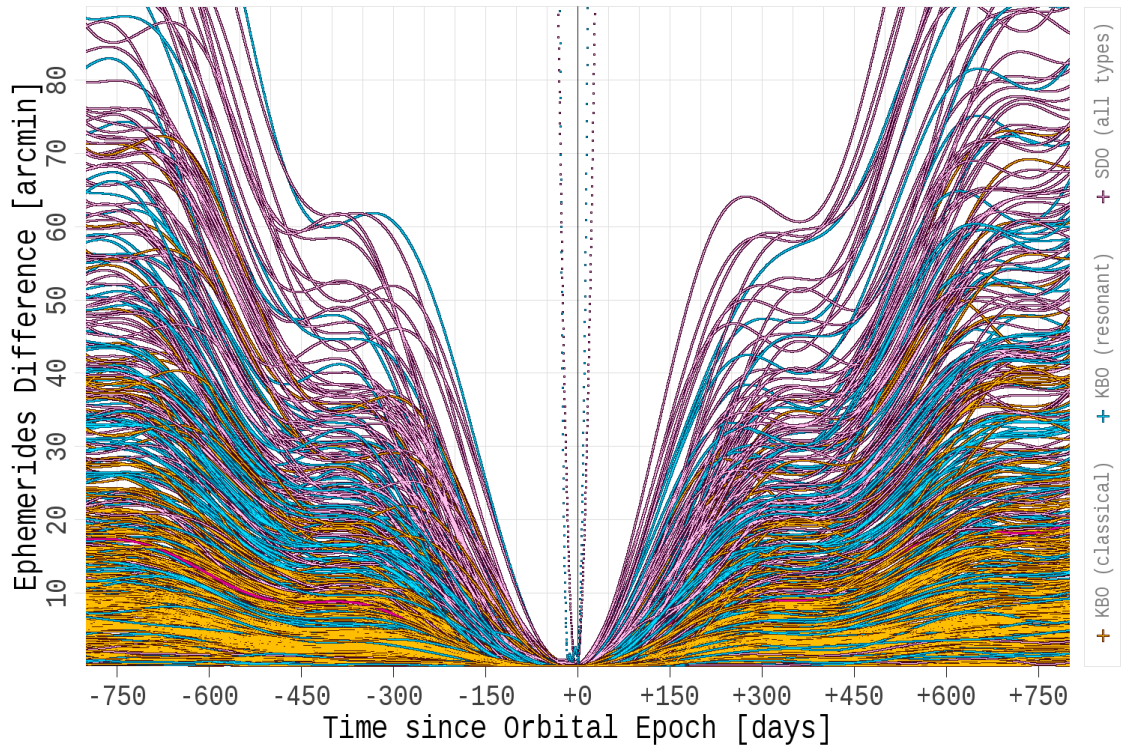


Fig. 4.— The difference between the ephemeris from the initial tracklet-pair orbit and the final orbit for all TNO events. Using a tracklet search radius of  $20'$  gives a  $\sim 250$  day window to find additional tracklets. The two events reaching an ephemeris error of  $\sim 90'$  within two weeks are due to particularly short arcs in the initial tracklet pairing.

The orbital elements of the identified objects were used to classify them as potential Trojans, classical or resonant TNOs, Scattered Disc Objects (SDOs), or Centaurs. The orbital elements were also used to identify known objects by comparing the location and position angle of all ephemerides at their orbit epoch to those computed using the Minor Planet Center (MPC) orbit catalogue after integration using Mercury6 (Chambers 1999). This method assumes the orbits from the MPC are more accurate than those identified in this study, which may not be true if our identified objects were independently previously observed by other telescopes over shorter orbital arcs.

### 3. Results and Discussion

The source catalogues used in this study span the time from 2010 Feb 24 to 2015 July 31, and are generated from 529 609 exposures in 61 065 pointings, with 93 799 429 652 total detections. The stationary source removal left 7 655 731 998 detections of which 232 447 038 were linked into 65 524 472 tracklets.

Figure 5 shows eccentricity vs semi-major axis for all identified objects, and we present a breakdown of these in Table 2, including the number of unknown and known objects, as well as the number expected (both total and to a limiting  $V = 22.5$ ) based on the MPC catalogue. We further discuss our identified objects in the following sections.

#### 3.1. Bright Objects

Brown et al. (2015) estimate that there is a 32% chance that a TNO having magnitude  $V < 19.1$  remains undiscovered after their archival search of the Catalina Sky Survey database. We computed ephemerides for the five year period of data used in this study, for all identified objects, and list the peak brightness of the top eight in Table 3. There is one



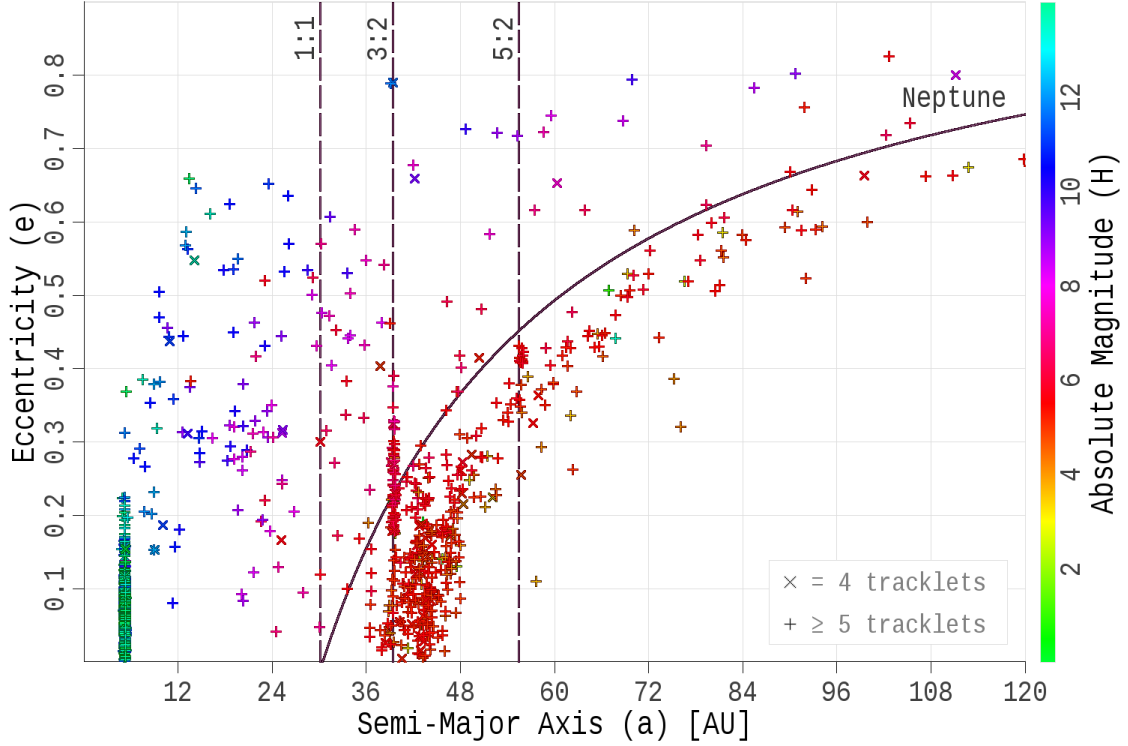


Fig. 5.— Eccentricity versus semi-major axis for the objects identified in this work, colour coded by absolute magnitude. The detected objects consist of 789 Jupiter Trojans, 154 Centaurs, and 465 total TNOs. The 1 : 1 and 3 : 2 mean motion resonances with Neptune are noted with vertical dashed lines, while Neptune’s aphelion distance of  $q = 30.4$  AU is noted with a solid curved line.

Table 2: Classification of identified objects, also broken down into known and unknown objects. The fifth column shows the expected number from the MPC catalogue as a fraction of the total for a limiting magnitude of  $V = 22.5$ .

orbital type	total	unknown	known	MPC ( $V < 22.5$ )	MPC total
Jupiter Trojans	789	145	644	6169	6207
Centaur	154	78	76	211	303
Classical TNOs	255	162	91	197	1198
Resonant TNOs	121	77	44	93	319
Scattered Disc	89	52	37	57	203

object which reaches  $V = 18.5$ , which is the third brightest TNO over the timespan of data used in this study.

### 3.2. Large Objects

Figure 6 plots semi-major axis vs absolute magnitude for all identified objects. The largest identified objects are all known, and are further listed in Table 4. However, (136472) Makemake and (134340) Pluto are not identified. For the first case, its tracklets do not occur within a 60 day window, and for the latter, the only tracklet pair occurred with a two day arc, and additional tracklets were not linked.

There are no unknown distant planetary-sized objects identified in our study. However, our minimum tracklet angular speed cut-off of  $0.001^\circ$  per day could exclude them if they are present in the source catalogues.

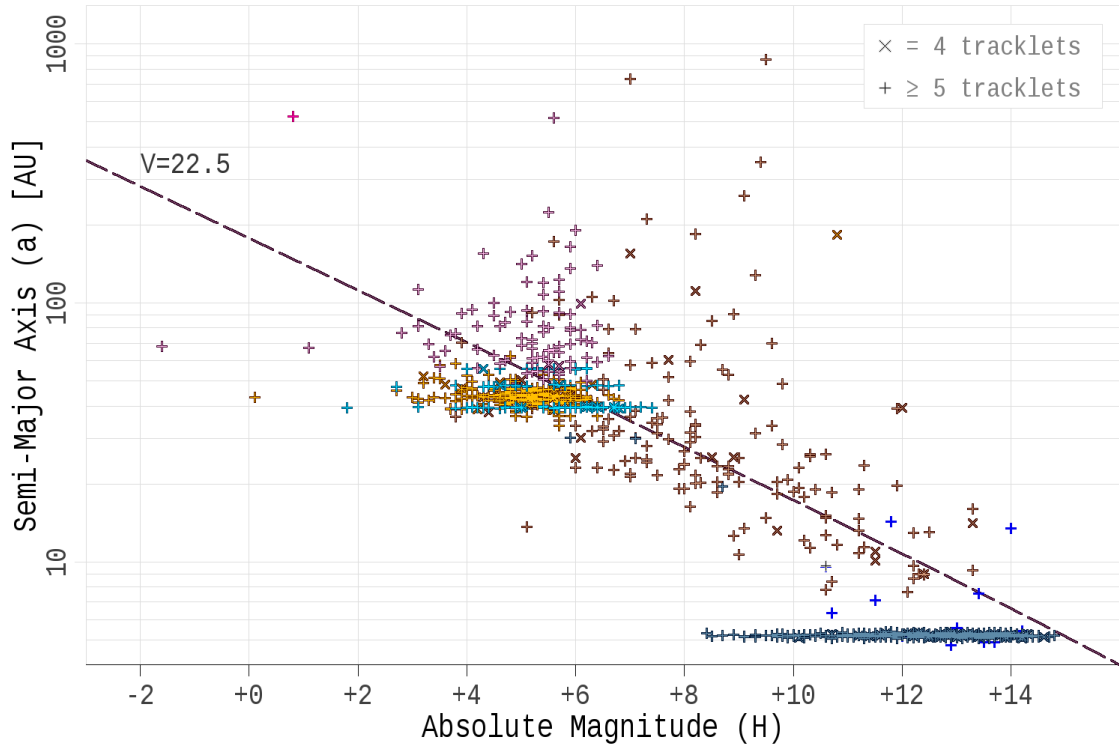


Fig. 6.— Semi-major axis vs absolute magnitude for all identified objects. The cluster along  $a \sim 5.2$  AU at the lower right are Jupiter Trojans. The largest objects (left most in the figure) are all known.

Table 3: The brightest eight objects (between 2010 Feb 24 and 2015 July 31) identified in our study. The first column gives the total tracklet count for each object. The magnitude column ( $V_{min}$ ) gives the brightest apparent  $V$  magnitude that each object reached during the five year PS1 survey data used based on the absolute magnitude ( $H$ ) determined from FindOrb, and  $N$  is the number of tracklets used for the orbit computation.

$N$	$a$ [AU]	$e$	$i$ [°]	$H$	$V_{min}$	object
13	43.2588	0.1905	28.193	0.1	17.2	(136108) Haumea
11	67.7662	0.4410	44.057	-1.6	18.2	(136199) Eris
11	36.2522	0.1894	1.497	3.8	18.5	<b>unknown</b>
12	39.4661	0.2182	20.554	1.8	18.6	(90482) Orcus
16	39.5548	0.2786	15.464	4.1	18.6	(38628) Huya
25	39.3913	0.2243	8.411	4.2	19.0	(47171) 1999 TC <sub>36</sub>
06	69.2813	0.5289	29.424	3.3	19.0	2010 EK <sub>139</sub>
16	41.3601	0.0193	19.307	3.1	19.2	(145452) 2005 RN <sub>43</sub>

### 3.3. Distant Objects

Figure 7 plots semi-major axis vs distance from the Sun (on 2015 July 31). The farthest of these objects are listed in Table 5, with the six most distant being known (including the recent 2015 RR<sub>245</sub><sup>3</sup>). In addition to these, we have identified two previously unknown objects which have perihelia well beyond the orbit of Neptune.

<sup>3</sup><http://www.minorplanetcenter.net/mpec/K16/K16N67.html>

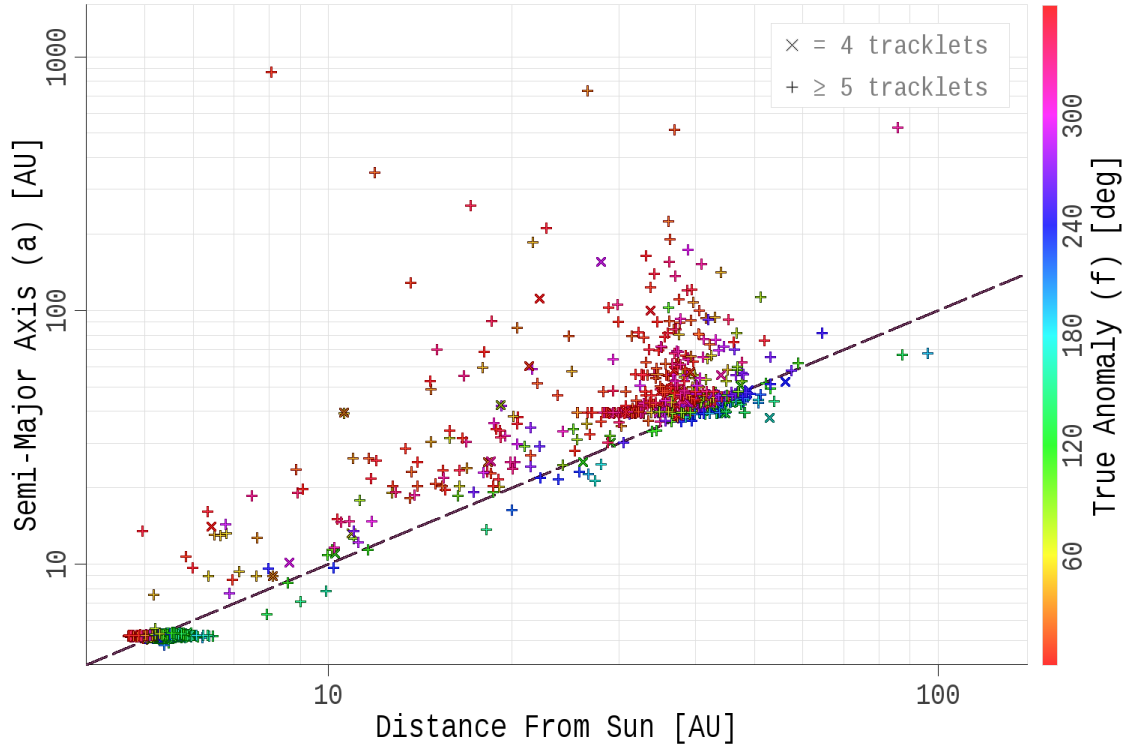


Fig. 7.— Semi-major axis vs distance from the Sun (on 2015 July 31) for all identified objects. The colour scheme shows the true anomaly, which gives a direct measure of where each object is along its orbit relative to perihelion. Objects significantly above the dashed line have much larger eccentricity, with comets being located towards the upper left of the plot.

Table 4: The most distant objects identified in our study. The column headings are identical to those given in Figure 3.

$N$	$a$ [AU]	$e$	$i$ [°]	$H$	$V_{min}$	object
11	67.7662	0.4410	44.057	-1.60	18.2	(136199) Eris
13	43.2588	0.1905	28.193	0.10	17.2	(136108) Haumea
12	525.8952	0.8554	11.929	0.80	20.1	(90377) Sedna
19	66.8888	0.5065	30.946	1.10	20.4	(225088) 2007 OR <sub>10</sub>
12	39.4661	0.2182	20.554	1.80	18.6	(90482) Orcus
18	45.7416	0.1402	21.497	2.70	19.4	(174567) Varda
11	47.5112	0.1304	24.337	2.70	19.3	(55565) 2002 AW <sub>197</sub>
11	76.5622	0.5186	23.344	2.80	19.2	(229762) 2007 UK <sub>126</sub>
13	43.1700	0.0506	17.154	3.00	19.4	(20000) Varuna
10	112.7967	0.6744	14.025	3.10	20.0	(303775) 2005 QU <sub>182</sub>
10	81.4754	0.5860	7.565	3.10	21.2	2015 RR <sub>245</sub>

### 3.4. Orbital Clustering

Batygin & Brown (2016) suggest the orbital configuration of TNOs decoupled from Neptune’s influence support the presence of a planetary-sized perturber in the outer solar system. Due to the sensitivity limit of PS1 ( $V \sim 22.5$ ), we can only identify two of these objects, namely (90377) Sedna and 2007 TG<sub>422</sub>, and both were identified in this study. We present the arguments of perihelia of our identified objects in Figure 8. Using a Kolmogorov-Smirnov test on all identified objects having  $q > 32$  AU and  $q > 36$  AU, we do not see clustering in  $\omega$ . To our sensitivity limit, this is significant as our wide field survey might be expected to have less observational bias than targeted narrow searches. Survey

Table 5: The most distant identified objects in our dataset, where  $r_{max}$  is their heliocentric distance on 2015 July 31. The first column ( $N$ ) gives the tracklet count for each object. Two of the identified objects are not known.

$N$	$a$ [AU]	$e$	$i$ [°]	$H$	$r_{max}$	object
11	67.7662	0.4410	44.057	-1.6	96.3	(136199) Eris
19	66.8888	0.5065	30.946	1.1	87.3	(225088) 2007 OR <sub>10</sub>
12	525.8952	0.8554	11.929	0.8	85.9	(90377) Sedna
10	81.4754	0.5860	7.565	3.1	64.5	2015 RR <sub>245</sub>
14	62.0774	0.3355	28.814	3.4	58.9	2015 KH <sub>162</sub>
07	57.7016	0.1103	46.604	3.5	57.5	2004 XR <sub>190</sub>
19	62.1612	0.2245	10.252	3.2	56.2	<b>unknown</b>
08	43.9118	0.2511	14.878	4.0	53.8	<b>unknown</b>

bias might also be expected to induce apparent clustering in an observed population, rather than remove it.

### 3.5. High Inclination Objects

From Figure 9, there are several identified objects with high inclination, and we list those having the largest inclination in Table 6. We identified in our study the recent 2011 KT<sub>19</sub><sup>4</sup>, and also have one unknown object with  $i = 84^\circ$ . The orbital evolution of highly-inclined TNOs is not understood, but Gladman et al. (2009) suggest they could have been perturbed into their current orbits by a planetary-sized perturber in the outer solar

---

<sup>4</sup>Minor Planet Circulars Orbit Supplement 380701

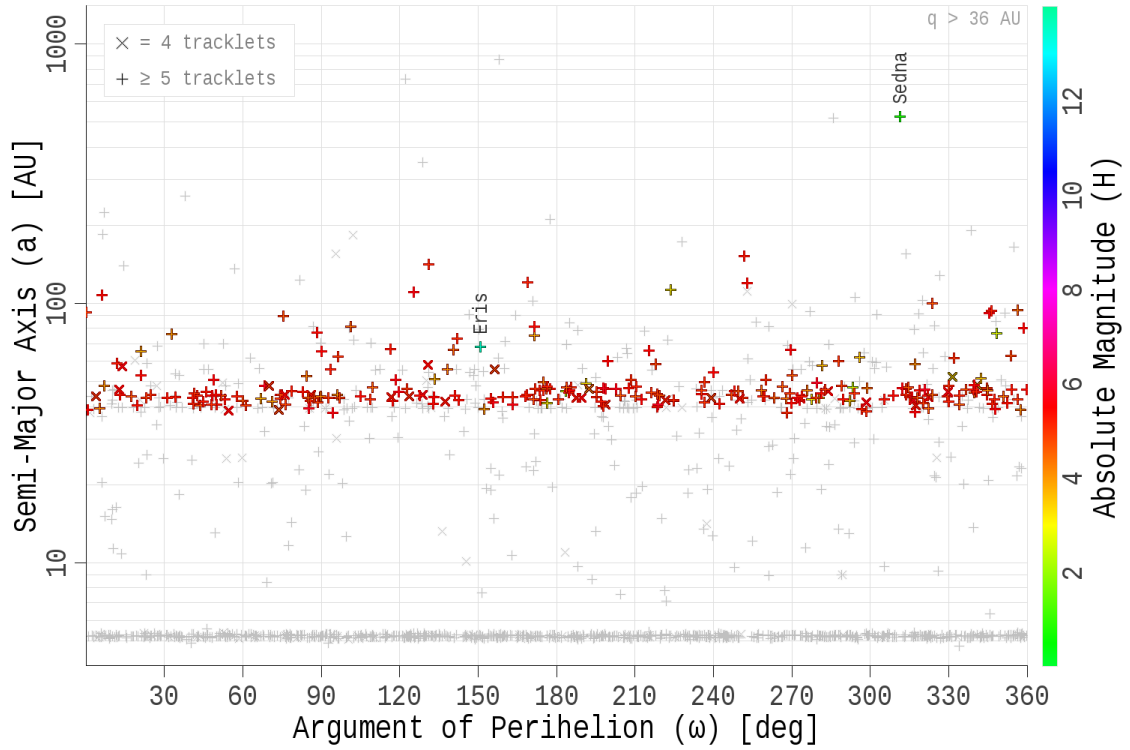


Fig. 8.— Semi-major axis versus argument of perihelion for all identified objects having  $q > 36$  AU. The location of (90377) Sedna and (136199) Eris are indicated. Sedna is the only object identified in this survey that supports the orbital clustering discussed in Trujillo & Sheppard (2014) and Batygin & Brown (2016).



system. Another plausible explanation is that they are captured objects.

Table 6: The identified objects (excluding comets) with highest inclination. The magnitude ( $V_{min}$ ) is the brightest each objects reaches over the five year data span used, and is determined from the absolute magnitude ( $H$ ) as fitted by FindOrb. The first column ( $N$ ) gives the number of tracklets used in the orbit computation.

$N$	$a$ [AU]	$e$	$i$ [°]	$H$	$V_{min}$	object
19	35.6490	0.3330	110.206	6.6	20.5	2011 KT <sub>19</sub>
06	259.7509	0.9354	84.824	9.1	21.5	<b>unknown</b>
06	349.2179	0.9685	68.030	9.4	20.0	(418993) 2009 MS <sub>9</sub>
06	39.4982	0.3899	54.265	6.5	20.6	<b>unknown</b>
10	43.3078	0.2160	47.507	6.0	21.3	<b>unknown</b>
07	57.7016	0.1103	46.604	3.5	21.1	2004 XR <sub>190</sub>

### 3.6. Neptune Trojans

We list in Table 7 two possible Neptune Trojans present in our identified objects, based solely on their orbital elements. One of these objects was identified in a parallel study using PS1 data (Lin et al. 2015), however we did not identify their other candidates. We present a discussion as to why this might be in Section 3.8.

### 3.7. Centaurs and Comets

We define Centaurs to have perihelia between Jupiter and Neptune, but which are not in a mean motion resonance with Neptune. We identified 136 Centaurs in our study, as well

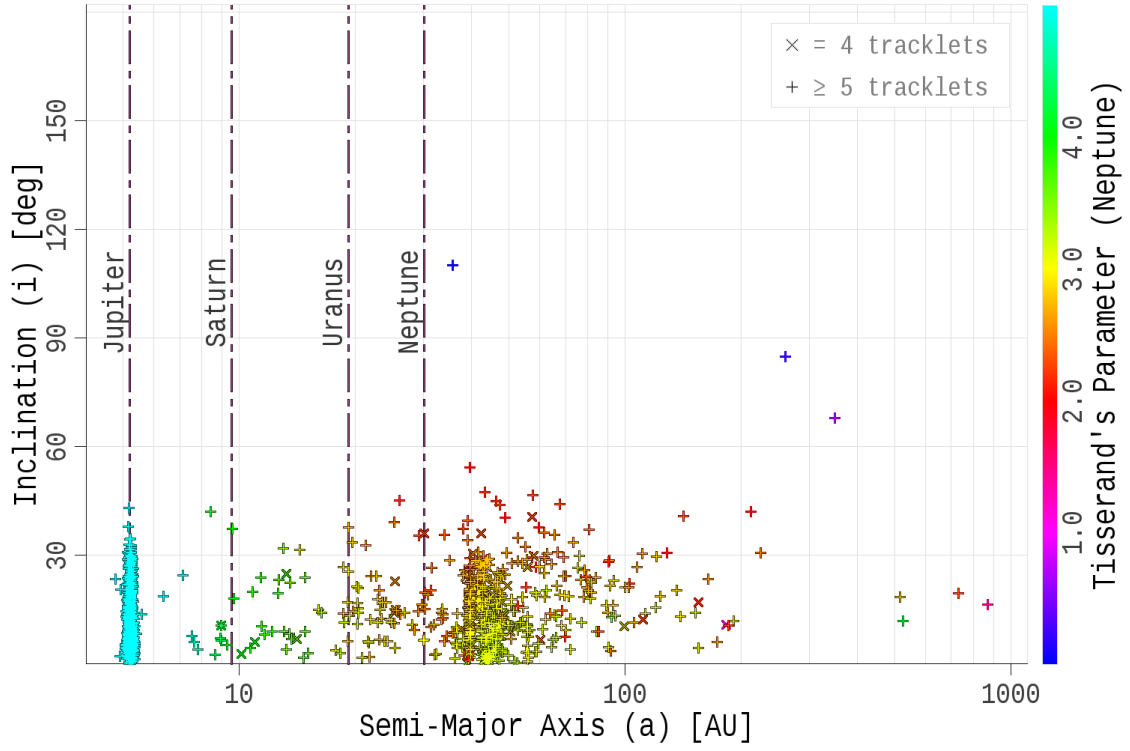


Fig. 9.— Inclination vs semi-major axis for all identified objects, colour coded by Tisserand’s parameter wrt. Neptune. The location of the giant planets are noted with vertical lines, with a large grouping of Jupiter Trojans towards the lower left. The identified object with highest eccentricity is known object 2011 KT<sub>19</sub>.

Table 7: Two possible Neptune Trojans (based on their orbital elements) identified. The first column ( $N$ ) indicates the number of tracklets used to compute the orbit.

$N$	$a$ [AU]	$e$	$i$ [°]	$H$	$V_{min}$	object
16	30.1564	0.1192	6.661	5.90	20.7	2013 KY <sub>18</sub>
06	30.0280	0.0472	6.562	7.10	21.6	2010 TS <sub>191</sub>

as 10 comets which were all known objects. Our identification method does not link objects having  $e \geq 1$ . Although Schlichting et al. (2013) call for a better characterised survey of Centaur objects, we consider them a by-product of the current study and leave this to a future publication — our primary interest here is identifying TNOs.

### 3.8. Identification Efficiency

Our discussion would not be complete without mentioning the efficiency of creating and pairing tracklets, as well as identifying additional tracklets. As suggested by Table 2, our method identifies about half of the expected (i.e., having  $V < 22.5$ ) known population of classical and resonant TNOs from the MPC catalogue, and two-thirds of the known SDOs. We do not count Jupiter Trojans or Centaur objects here because our detection parameters were empirically chosen to optimise detection of TNOs.

A complete end-to-end measure of the identification efficiency could be made by injecting synthetic detections into our software routines (e.g., as is done by MOPS; Denneau et al. 2013), but ideally this must be done directly into the original PS1 image data which would then be used to produce new source catalogues. This reprocessing by the IPP (Magnier 2006) is necessary for a realistic efficiency determination as the fill-factor of the

PS1 camera is limited to  $\sim 70\%$ , and our tracklet linking routines have no knowledge of which regions on the CCD are masked. Also, our limiting sensitivity is dependent on the photometric passband as well as local weather conditions. Because of these reasons, determining an accurate efficiency is a significant undertaking, which we will address in subsequent work to obtain an unbiased estimate of the true TNO population.

From the current MPC catalogue for all known objects, the average distance between each asteroids within  $30^\circ$  of the ecliptic and its closest neighbour having apparent magnitude within 0.4 is  $\sim 820''$ . This is much greater than the  $16''$  search radius used during the tracklet creation process, suggesting that the majority of tracklets in the source catalogue (after removing stationary sources) will not be contaminated by detections associated with different objects. Our tracklets may be limited in terms of their RMS residual, but even for a distant object at 100 AU, detections will be spaced  $0.45''$  for a 20 minute TTI, which is twice the PS1 pixel scale.

Because Figure 4 suggests additional tracklets should be readily found, this implies the efficiency of our search implementation is limited by either the stationary source removal process, or the tracklet pairing stage. We also note that while the PS1 camera fill-factor may lead to missed detections for NEOs, it can result in completely missed tracklets for TNOs due to their much slower speed across the celestial sphere.

#### 4. Conclusions

A search for distant objects was made using the archival PS1 data, with 1420 objects identified, consisting of 255 classical TNOs, 121 resonant TNOs, 89 SDOs, 154 Centaurs, and 789 Jupiter Trojans. Excluding the trojans, 371 of these are new objects which we could not link to known objects.

While our identified objects do not show a clustering in their arguments of perihelia, increasing the number of known retrograde TNOs and Sedna-like SDOs is important in better understanding the distant population in our solar system, especially to constrain the orbital elements and mass of any potentially undiscovered large planetary-sized objects (Trujillo & Sheppard 2014; Batygin & Brown 2016).

Future work will focus on validating the detection efficiency, as well as optimising our detection parameters to work well beyond the classical TNO regime.

### **Acknowledgments**

The Pan-STARRS1 Surveys (PS1) have been made possible through contributions of the Institute for Astronomy, the University of Hawaii, the Pan-STARRS Project Office, the Max-Planck Society and its participating institutes, the Max Planck Institute for Astronomy, Heidelberg and the Max Planck Institute for Extraterrestrial Physics, Garching, The Johns Hopkins University, Durham University, the University of Edinburgh, Queen’s University Belfast, the Harvard-Smithsonian Center for Astrophysics, the Las Cumbres Observatory Global Telescope Network Incorporated, the National Central University of Taiwan, the Space Telescope Science Institute, the National Aeronautics and Space Administration under Grant Nos. NNX08AR22G, NNX12AR65G, and NNX14AM74G issued through the Planetary Science Division of the NASA Science Mission Directorate, the National Science Foundation under Grant No. AST-1238877, the University of Maryland, and Eotvos Lorand University (ELTE) and the Los Alamos National Laboratory.

## REFERENCES

- Alexandersen, M., Gladman, B., Kavelaars, J. J., et al. 2014, ArXiv e-prints, arXiv:1411.7953
- Batygin, K., & Brown, M. E. 2016, *AJ*, 151, 22
- Bernstein, G. M., Trilling, D. E., Allen, R. L., et al. 2004, *AJ*, 128, 1364
- Brown, M. E., Bannister, M. E., Schmidt, B. P., et al. 2015, ArXiv e-prints, arXiv:1501.00941
- Chambers, J. 1999, *MNRAS*, 304, 793
- de la Fuente Marcos, C., de la Fuente Marcos, R., & Aarseth, S. J. 2015, *MNRAS*, 446, 1867
- Denneau, L., Jedicke, R., Grav, T., et al. 2013, *PASP*, 125, 357
- Elliot, J. L., Kern, S. D., Clancy, K. B., et al. 2005, *AJ*, 129, 1117
- Fraser, W. C. 2009, *ApJ*, 706, 119
- Fuentes, C. I., & Holman, M. J. 2008, *AJ*, 136, 83
- Gladman, B., Kavelaars, J. J., Petit, J.-M., et al. 2001, *AJ*, 122, 1051
- Gladman, B., Kavelaars, J., Petit, J.-M., et al. 2009, *ApJ*, 697, L91
- Gladman, B., Lawler, S. M., Petit, J.-M., et al. 2012, *AJ*, 144, 23
- Jewitt, D., & Luu, J. 1993, *Nature*, 362, 730
- Kaiser, N. 2004, in Society of Photo-Optical Instrumentation Engineers (SPIE) Conference Series, Vol. 5489, Society of Photo-Optical Instrumentation Engineers (SPIE) Conference Series, ed. J. M. Oschmann, Jr., 11–22
- Kozai, Y. 1962, *AJ*, 67, 591

- Kubica, J., Denneau, L., Grav, T., et al. 2007, *Icarus*, 189, 151
- Larsen, J. A., Gleason, A. E., Danzl, N. M., et al. 2001, *AJ*, 121, 562
- Larson, S., Beshore, E., Hill, R., et al. 2003, in *Bulletin of the American Astronomical Society*, Vol. 35, AAS/Division for Planetary Sciences Meeting Abstracts #35, 982
- Larson, S., Brownlee, J., Hergenrother, C., & Spahr, T. 1998, in *Bulletin of the American Astronomical Society*, Vol. 30, *Bulletin of the American Astronomical Society*, 1037
- Lin, H.-W., Chen, Y. T., Holman, M. J., & Ip, W.-H. 2015, in *AAS/Division for Planetary Sciences Meeting Abstracts*, Vol. 47, AAS/Division for Planetary Sciences Meeting Abstracts, 211.17
- Magnier, E. 2006, in *The Advanced Maui Optical and Space Surveillance Technologies Conference*
- Morbidelli, A., Bottke, W. F., Nesvorný, D., & Levison, H. F. 2009, *Icarus*, 204, 558
- Petit, J.-M., Holman, M. J., Gladman, B. J., et al. 2006, *MNRAS*, 365, 429
- Petit, J.-M., Kavelaars, J. J., Gladman, B., & Loredó, T. 2008, *Size Distribution of Multikilometer Transneptunian Objects*, ed. M. A. Barucci, H. Boehnhardt, D. P. Cruikshank, A. Morbidelli, & R. Dotson, 71–87
- Schlichting, H. E., Fuentes, C. I., & Trilling, D. E. 2013, *AJ*, 146, 36
- Schlichting, H. E., Ofek, E. O., Sari, R., et al. 2012, *ApJ*, 761, 150
- Shankman, C., Gladman, B. J., Kaib, N., Kavelaars, J. J., & Petit, J. M. 2013, *ApJ*, 764, L2
- Sheppard, S. S., & Trujillo, C. A. 2010, *ApJ*, 723, L233

Sheppard, S. S., Udalski, A., Trujillo, C., et al. 2011, *AJ*, 142, 98

Trujillo, C. A., & Sheppard, S. S. 2014, *Nature*, 507, 471

Wainscoat, R., et al. 2015, in *IAU Symposium 318*, ed. S. Chesley & R. Jedicke, 293